e-ISSN: 2582-5208
International Research Journal of Modernization in Engineering Technology and Science
(Peer-Reviewed, Open Access, Fully Refereed International Journal)
Volume:05/Issue:10/October-2023 Impact Factor- 7.868 www.irjmets.com

ELECTRO-DETURBIDIZATION OF CRUDE OIL POLLUTED WATER USING ALUMINIUM ELECTRODE

John C. Igwe*1, Matthew C. Menkiti*2, Victor I. Ugonabo*3

*1,2,3Department Of Chemical Engineering, Nnamdi Azikiwe University, Awka.

DOI : https://www.doi.org/10.56726/IRJMETS45217

ABSTRACT

Deturbidization of crude oil-polluted water by electrocoagulation was investigated using an aluminium (Al) electrode. The crude oil used in this experiment was obtained from the shell petroleum development company (SPDC) flow station at Kokori in Ethiope East local government area of Delta state. The experiment was performed in a batch electrochemical cell with an aluminium electrode in a monopolar connection. To estimate the efficiency of the electrocoagulation technique, preliminary tests were conducted. And the best result was achieved at pH 8, the current dosage of 2.5A, a temperature of 298 K, and contact time of 30 min. With a turbidity removal efficiency of 84.7%. The data obtained were analysed using the pseudo-first-order, pseudo-second-order, Elovich, intra-particle diffusion, and the Boyd kinetic models. Using the regression coefficient (r^2), the kinetic rates conformed to the pseudo-second-order kinetic model. The result were further analysed using different adsorption isotherms such as: Freundlich, Temkin, Langmuir, and Dubinin-Radushkevich (D-R) model. And the sorption process was found to fit best with the Langmuir adsorption isotherm with monolayer coverage of adsorbed molecules. The thermodynamics study shows that the adsorption process was endothermic and spontaneous.

Keywords: Electrocoagulation, Deturbidization, Adsorption Kinetics, Isotherm, Thermodynamics.

I. INTRODUCTION

The high percentage of turbidity in crude oil-polluted water has become an environmental issue today. Its reduction before discharge to the water body constitutes a challenge and a source of concern. Petroleum produces water that contains a lot of toxic contaminants with high turbidity which prevents oxygen dissolution [1]. Petroleum-produced water is characterized by contaminants such as oil, ammonia, benzene, sulfide, chloride, phosphate, cyanide, heavy metals, phenols, high BOD and COD among other toxic pollutants. In electrocoagulation, the coagulant is generated in situ through the dissolution of the sacrificial anode by applying either a direct (d.c) or an alternate (a.c) current between the anode and cathode electrodes. However, the efficiency of the electrocoagulation process depends on factors such as current density, electrolysis time, initial pH, and temperature.

An EC system is simply an electrolytic cell which involves the passage of current source that is connected to at least one anode and cathode submerged in an electrolyte. The electrolyte, which is the water or wastewater that is to be treated, completes the electrical circuit by allowing charges to migrate between the electrodes. The pollutant is generally adsorbed at the surface of the flocs (coagulant) generated electrochemically. According to Balasubramanian, et al., (2009), critical analysis of the electrocoagulation of pollutants reveals that there are two separate processes taking place (a) the electrochemical process through which the metal coagulants are generated Physio-chemical process through which the effluents are adsorbed on the surface of the coagulants. The electrocoagulation process does not require the addition of a chemical coagulant. Instead, it is generated by oxidation of the anode material when electricity is passed through the electrodes. Current is applied to promote the generation of metal cations at the anode, and the evolution of hydrogen gas at the cathode (Bagga, et al., 2008; Inan et al., 2004; Zhu and Ahn, 2005).

In Electrocoagulation method, the commonly used electrodes are aluminium [2] and iron [3]. The use of platinum [4; 49] stainless steel [5; 6], and titanium [7] electrodes have also been reported. In the electrocoagulation process, current is passed through the electrode (oxidation of anode) which dissolves to form ions and subsequent production of metallic hydroxide $Mn(OH)_n$ at the cathode. The aluminium hydroxide species generated are responsible for the flocculation and agglomeration of contaminants. Electrocoagulation is an efficient process in treating contaminated wastewater such as textile wastewater [9], industrial wastewater,

e-ISSN: 2582-5208
International Research Journal of Modernization in Engineering Technology and Science
(Peer-Reviewed, Open Access, Fully Refereed International Journal)
Volume:05/Issue:10/October-2023 Impact Factor- 7.868 www.irjmets.com

wastewater containing arsenic [10], phenolic compounds [11], heavy metals [12], pulp and paper mill wastewater [13], petrochemical industry wastewater [14], oil suspension [15], and fluorides [16]. Electrocoagulation has been successfully applied to the treatment of various types of wastewater but its application in the treatment of crude oil-contaminated wastewater is still scarcely available in the literature.

The advantages of electrocoagulation include high particulate removal efficiency, relatively low cost, and the requirement of simple equipment. This method is characterized by reduced sludge production, a minimum requirement of chemicals and ease of operation [17].

In this respect, our aims through this work were to:

- The experiment aims to evaluate each process and generate important design kinetic and isotherm parameters.
- To investigate the possibility of using electro-coagulation technology for the treatment of crude oil-contaminated water using aluminium (Al) electrodes.
- To evaluate the process parameters and characterize the produced water received.
- The research will also focus on understanding the mechanisms involved in the process.

II. RESEARCH METHODOLOGY

2.1. Material collection and preparations

The crude oil used in this experiment was collected from the shell petroleum development company (SPDC) flow station at Kokori in the Ethiope East local government area of Delta State. The crude oil was simulated in batches, depending on the operating parameters considered by mixing either 25mg/L, 50mg/L, 75mg/L, 100mg/L or 125mg/L of crude oil in 500ml of distilled water.

2.2 Experimental Device and Apparatus

The experimental set-up shown in Figure 1 consists mainly of an electrocoagulation reactor, a magnetic stirrer with a hot plate, a d.c power supply and a pair of aluminium electrodes (as anode and cathode). Others include a nephelometric turbidity meter (Elico CL52D), pH meter (Delta 320m), beakers, Whatman no 42 (125mm) filter paper, separating funnel, conical flask, stopwatch, measuring cylinder, syringe, weighing balance, turbidity meter, crude oil, distilled water, potassium chloride (KCl),

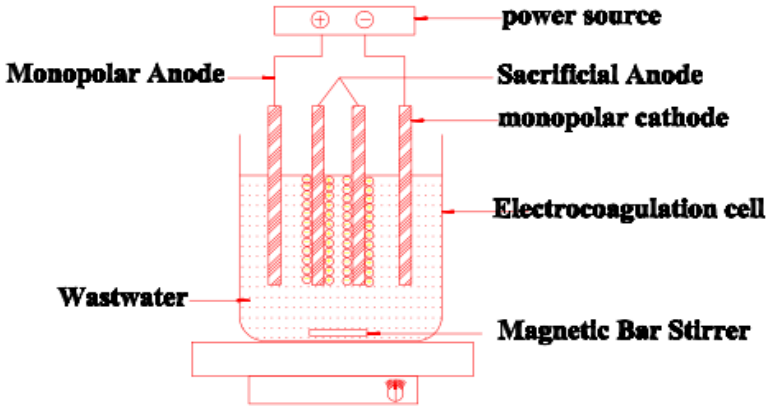

Fig. 1. Schematic diagram of EC cell

2.3. Electrocoagulation procedure

The electrocoagulation experiment was carried out in a 500 mL beaker. In each run, the beaker was filled with 250 mL of synthetic emulsion (produce water) and placed on a magnetic stirrer for homogeneity. A pair of Al electrodes were used as an anode and cathode. The electrodes were connected to a d.c source and immersed vertically into the beaker with an inter-electrode distance of 3 cm and electrode surface area of 2.64 cm^2 (3.84cm x 0.69 cm). The initial pH value of the sample was adjusted to the desired value using 1.0 mol/L NaOH and HCl. While the current and voltage flowing through the electrodes were measured with an ammeter and voltmeter, respectively. Potassium chloride (KCl) was added to each sample to maintain the conductivity. The conductivity and temperature of the sample were measured using a turbidity meter (Lovibond Senso Direct Con 2000) and thermometer, respectively.

e-ISSN: 2582-5208
International Research Journal of Modernization in Engineering Technology and Science
(Peer-Reviewed, Open Access, Fully Refereed International Journal)
Volume:05/Issue:10/October-2023 Impact Factor- 7.868 www.irjmets.com

After each run, the sample was allowed to sediment for 900s (15 min). After which, an aliquot of 10 mL was drawn from the mid-depth of the beaker and analysed for turbidity using a nephelometric turbidity meter. The electrode surfaces were cleaned by dipping them into Acetone for the 60s and rinsed with distilled water to remove any solid residues on the surface.

Eq. 1 is an expression used to calculate the percentage turbidity removal efficiency.

$$R\% = \frac{C_i - C_f}{C_i} \times 100 \quad (1)$$

Where C_i and C_f are the pollutant turbidity before and after the electrocoagulation experiment respectively, R% is the removal efficiency. The value of the turbidity NTU (Nephelometric Turbidity Unit) obtained was converted to concentration (mg/L) by multiplying with 2.3 [18].

The experiment was repeated at different pH, current density, time and temperature.

2.4. Theoretical Principles

2.4.1. Adsorption Kinetics

The kinetics of pollutant removal is explicitly explained in the literature using different models.

The adsorption capacity q_t (mg/g) at time t was determined using the below equation [19]:

$$q_t = \frac{v(C_o - C_t)}{w} \quad (2)$$

Where v is the volume of the solution in a litter, w is the mass of the adsorbate in gram, Co is the initial concentration of the adsorbent at time zero and C_t is the concentration of the adsorbent at the end of time t in mg/L.

The amount of pollutant adsorbed at equilibrium on electrode species q_e (mg/g) was calculated from the following equation [20].

$$q_e = \frac{v(C_o - C_e)}{w} \quad (3)$$

Where Ce is the solution concentration at equilibrium.

Pseudo-first-order kinetic model

The pseudo-first-order kinetic model can be described using the below equation [20]:

$$\frac{dq}{q_t} = K_1(q_e - q_t) \quad (4)$$

The integrated form of Eq. (4) with the boundary conditions t = 0 to t = t and q = 0 to q = q_t becomes:

$$q_t = q_e[1 - exp(-K_1 t)] \quad (5)$$

Eq. 5 is the nonlinear form of the pseudo-first-order kinetic model, q_e and q_t are the amount of pollutant adsorbed at equilibrium and time t, respectively (mg/g), and k_1 is the rate constant of first-order adsorption (s^{-1}).

Eq. (5) can be rearranged to obtain the linear form of the pseudo-first-order model,

$$log(q_e - q_t) = log(q_e) - \frac{K_1 t}{2.303} \quad (6)$$

k_1 and q_e values are obtained from the slope and intercept of the plot of log (q_e-q_t) against t.

Pseudo-second-order kinetic model

The pseudo-second-order kinetic equation can be expressed using the below equation [21]:

$$\frac{d_q}{d_t} = K_2(q_e - q_t)^2 \quad (7)$$

The integrated form of Eq. (7) with boundary conditions t = 0 to t = t, q = 0 to q = q_t becomes:

$$\frac{1}{q_e - q_t} = \frac{1}{q_e} + K_2 t \quad (8)$$

On further rearrangement, Eq. (8) becomes:

$$q_t = \frac{K_2 q_e^2 t}{1 + q_e K_2 t} \quad (9)$$

The linearized form of Eq. (9) is as follows:

$$\frac{t}{q_t} = \frac{1}{K_2 q_e^2} + \frac{t}{q_e} \quad (10)$$

e-ISSN: 2582-5208
International Research Journal of Modernization in Engineering Technology and Science
(Peer-Reviewed, Open Access, Fully Refereed International Journal)
Volume:05/Issue:10/October-2023 Impact Factor- 7.868 www.irjmets.com

where k_2 (s^{-1}) is the rate constant of second-order adsorption. The pseudo-second-order kinetic plot of t/q_t versus t produced the equilibrium adsorption capacity q_e, and the second-order rate constant k_2 from the slope and intercept, respectively.

Elovich kinetic model

The Elovich kinetic model can be described using Eq. 11 [16]. It is based on the kinetic principle that assumes that the active adsorption sites increase exponentially, implying multilayer surface adsorption [Rania and Yousef, 2015]. The Elovich model may be written as [23; 24].

$$\frac{d_{qt}}{d_t} = \alpha e^{-\beta q_t} \quad (11)$$

On integration of Eq. 11 with the same boundary conditions as pseudo-first and second-order kinetic equations, we have Eq. 12:

$$q_t = \frac{1}{\beta} In(\alpha\beta) + \frac{1}{\beta} In(t) \quad (12)$$

α is the initial adsorption rate (mg/s), and β is the desorption constant (g/mg). The Elovich constants α and β were obtained through the slope and intercept of a plot of q_t against In t.

Intra-particle diffusion

To investigate the mechanism of pollutant adsorption onto the electrode, intra-particle diffusion was applied to further analyse the experimental data. The Intra-particle diffusion model can be described using Eq. 13 [18]. It is proposed that the uptake of the adsorbate by the adsorbent varies almost proportionately with the square root of time ($t^{1/2}$) [26].

$$q_t = K_d\sqrt{t} + \theta \quad (13)$$

q_t is the amount of pollutant adsorbed per unit mass of adsorbent (mg/g) at a time t and K_d is the intra-particle diffusion rate constant ($mg/g.s^{-1/2}$). The amount of sorbate sorbed q_t, was plotted against the square root of time $t^{1/2}$, from which the rate constant k_d, and boundary layer thickness θ, was determined through the slope and intercept, respectively.

To further understand the mechanism of the adsorption process, the experimental data were further analysed using the Boyd-Reichenberg kinetic model described by Eq. 14 [32; 33]:

$$F = 1 - \frac{6}{\pi^2} exp(-B_t) \quad (14)$$

$$F = \frac{q_t}{q_e} \quad (15)$$

Where, F is the fraction of metal ions adsorbed at any time t, and B_t is a mathematical function of F.

$$B_t = -0.4977 - In(1 - F) \quad (16)$$

2.4.2 Adsorption isotherm

Many theoretical models have been developed in the literature, but for the purpose of this study; the Langmuir, Freundlich, Temkin and Dubinin-Radushkevich (D-R) isotherm was applied to determine the best fit isotherm. Since the amount of coagulant can be estimated stoichiometrically for a given time, the pollutant removal can be modelled by the adsorption phenomenon [10].

Table 1: Used linear and nonlinear isotherm equations.

Isotherm	Linear	Nonlinear	Reference
Langmuir	$\frac{C_e}{q_e} = \frac{1}{q_o b} + \frac{C_e}{q_o}$	$q_e = \frac{Q_m K_L C_e}{1 + K_L C_e}$	[35]
D-R	$Inq_e = Inq_s - 2\beta\varepsilon^2$	$q_e = q_s exp(-2\beta\varepsilon^2)$	[36]
Temkin	$q_e = BlogA + BlogC_e$	$q_e = B\ log\ AC_e$	[37]
Freundlich	$log(q_e) = log(k_f) + \frac{1}{n} log(C_e)$	$q_e = k_f C_e^{1/n}$	[38]

e-ISSN: 2582-5208
International Research Journal of Modernization in Engineering Technology and Science
(Peer-Reviewed, Open Access, Fully Refereed International Journal)
Volume:05/Issue:10/October-2023 Impact Factor- 7.868 www.irjmets.com

2.4.3 Adsorption thermodynamics

Thermodynamic parameters such as entropy change (ΔS^0), enthalpy change (ΔH^0) and Gibb's free energy (ΔG^0) were evaluated according to Eqs. 17 and 18 [44].

$$\Delta G = -RTInb \quad (17)$$

$$Inb = \frac{\Delta S}{R} - \frac{\Delta H}{RT} \quad (18)$$

Where R is the gas constant (kJ/mol.K), and T is the temperature (K).

2.4.4. Mean energy of adsorption (E_a)

The mean energy of adsorption (E_a, kJ/mol) which provides information about the adsorption mechanism was calculated from Eq. 19 [46].

$$E_a = \frac{1}{\sqrt{2\beta}} \quad (19)$$

The constant β ($mol^2.K/J^2$) was determined from the Dubinin-Radushkevich isotherm model.

III. RESULTS AND DISCUSSION

3.1. Adsorption kinetics

Figs. 2 and 3 (linear and nonlinear) present the fitted data onto pseudo-first-order kinetic according to Eqs. 4 and 5. The model parameters were shown in Table 2. The regression coefficient (r^2) suggested that the nonlinear form of the pseudo-first-order kinetic model gives a better fit when compared to the linear form. It was observed that the pseudo-first-order model does not fit the adsorption process. Since the equilibrium adsorption capacity q_e obtained experimentally does not agree perfectly well with the calculated q_e values, this suggested that the adsorption process does not follow pseudo-first-order kinetics.

The appropriate model that best describes the adsorption process was chosen based on the regression coefficient (r^2) and the nearness of the experimental equilibrium adsorption capacity q_e to the calculated q_e values. Figs. 4 and 5 show the results of the kinetic adsorption studies for linear and nonlinear pseudo-second-order models. From Table 3, both the linear and nonlinear models showed high regression coefficient (r^2) with negligible difference between the experimental and calculated q_e values. From the data obtained, both linear and nonlinear pseudo-second-order kinetic model fits into the adsorption process but the nonlinear model produced much better results when compared to the linear. This is mainly because transforming a nonlinear kinetic model to a linearized form tends to alter the error distribution, and thus distort the parameters [22].

The obtained constants, the regression coefficient (r^2) for both linear and nonlinear Elovich kinetic models were shown in Table 4. The experiment shows that the kinetic parameters (β, α) obtained for both linear and nonlinear methods vary with the initial concentration. The variation implies that the adsorption process is more than one mechanism [6; 25]. The regression coefficient (r^2) value showed that the nonlinear (Fig. 7) method provided a better description of the electrocoagulation process than the linear (Fig. 6). It is evident that the kinetic curve simulated by the Elovich model does not produce a better description of the adsorption process when compared to the pseudo-second-order model.

Fig. 8 shows a graphical plot of q_t versus $\sqrt{t}$ (according to Eq. 13) at different initial concentrations. If a linear plot of q_t against $t^{1/2}$ passes through the origin, intra-particle diffusion is the only rate-controlling step. If not, some other mechanisms are involved [27]. It is noticed from Fig. 5, that the graph does not pass through the origin which can be attributed to the difference between the rate of mass transfer in the initial and final stages of the adsorption process [Karthikeyan et al., 2005]. The above assertion is an indication that intra-particle diffusion is not the only rate-controlling step. Table 5 displays the intra-particle model parameters (k_d, θ and r^2) for the electro-determinization of crude oil-polluted water using the aluminium electrode. The k_d values increase with the increase in initial concentration. The increase in concentration also increases the driving force for diffusion of sorbate molecules into the pores of the adsorbent which is evident in higher k_d values [29; 30; 31].

Using the Boyd model according to (Eqs. 14, 15 and 16), B_t was plotted against t as shown in Fig. 9. The linearity of the plot indicated that external mass transfer is the main rate-controlling step at the initial stages of the adsorption process. It's also an indication that to some degree, film diffusion will control the sorption process

e-ISSN: 2582-5208
International Research Journal of Modernization in Engineering Technology and Science
(Peer-Reviewed, Open Access, Fully Refereed International Journal)
Volume:05/Issue:10/October-2023 Impact Factor- 7.868 www.irjmets.com

confirming that intra-particle diffusion is not only the rate-limiting step. Similar work was also reported by [34] on solid-liquid adsorption for wastewater treatment.

Table 2: pseudo first order kinetic parameters.

		Linear			nonlinear		
C_i (mg l^{-1})	$q_{e,exp}$(mg g^{-1})	q_e (mg g^{-1})	k_1 (s^{-1})	r^2	q_e (mg g^{-1})	k_1 (s^{-1})	r^2
25	386.6	407.1986	6.9E-4	0.9805	392.0988	3.19920E-4	0.9795
50	356.5	329.3100	6.9E-4	0.9782	349.5990	2.97317E-4	0.9887
75	377.1	393.6400	6.9E-4	0.9772	378.4990	2.17317E-4	0.9945
100	297.5	267.5900	4.6E-4	0.8771	302.5988	1.87317E-4	0.9678
125	289.3	260.8200	4.6E-4	0.8703	259.8200	1.27317E-4	0.9467

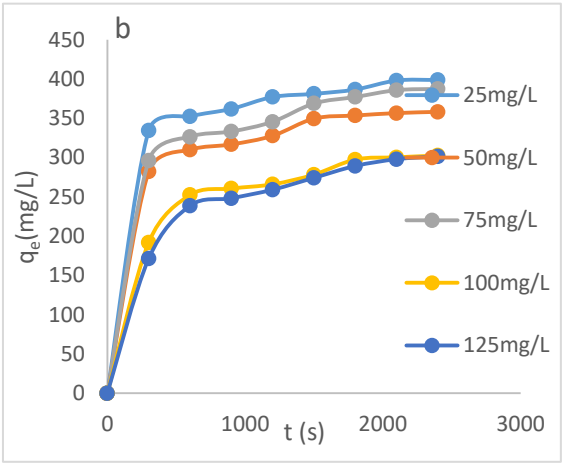

Fig. 2. Nonlinear Pseudo first-order kinetic.

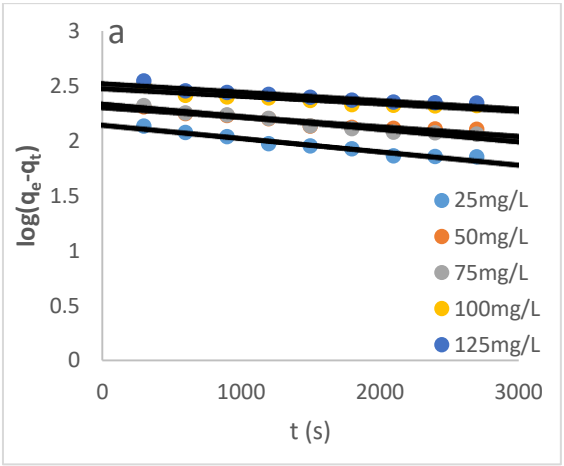

Fig. 3. Linear Pseudo first-order kinetic.

e-ISSN: 2582-5208
International Research Journal of Modernization in Engineering Technology and Science
(Peer-Reviewed, Open Access, Fully Refereed International Journal)
Volume:05/Issue:10/October-2023 Impact Factor- 7.868 www.irjmets.com

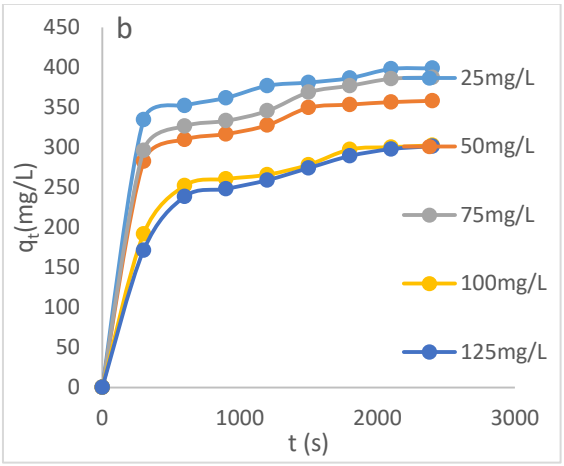

Fig. 4. Nonlinear Pseudo second-order kinetic.

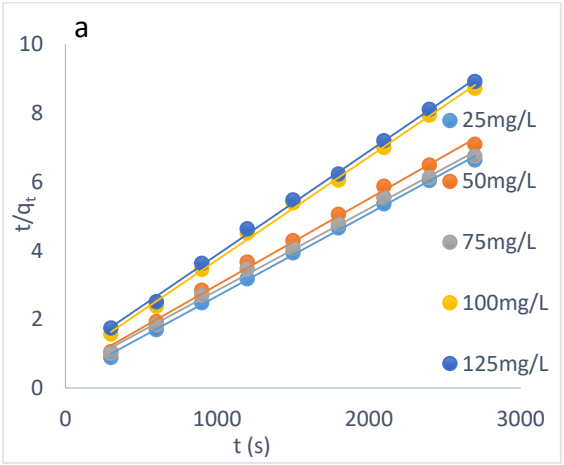

Fig. 5. Linear Pseudo second-order kinetic.

Table 3: Pseudo second-order kinetic

		Linear			nonlinear		
C_i (mg l^{-1})	$q_{e,\,exp}$(mg g^{-1})	q_e (mg g^{-1})	k_2 (s^{-1})	r^2	q_e (mg g^{-1})	k_2 (s^{-1})	r^2
25	386.6	380.09	3.1E-5	0.9988	386.5989	3.5E-5	0.9998
50	356.5	358.07	2.1E-5	0.9965	356.4988	1.1E-5	0.9965
75	377.1	380.66	1.9E-5	0.9969	377.0991	1.1E-5	0.9978
100	297.5	299.18	1.4E-5	0.9978	297.499	0.9E-5	0.996
125	289.3	290.99	1.0E-5	0.9986	289.2993	0.7E-5	0.9985

Table 4: Elovich kinetic parameters.

	linear			nonlinear		
C_i (mg l^{-1})	$\frac{1}{\beta}$	α (mg g^{-1} s^{-1})	r^2	$\frac{1}{\beta}$	α (mg g^{-1} s^{-1})	r^2
25	32.0	3315.5	0.9897	29.0	5312.5	0.9957
50	43.67	82.380	0.9837	76.01	183.84	0.9890
75	47.01	76.010	0.9673	84.50	98.210	0.9736
100	50.25	264.30	0.9577	49.53	310.33	0.9668
125	555.6	6448.9	0.9644	510.4	434.92	0.9588

e-ISSN: 2582-5208
International Research Journal of Modernization in Engineering Technology and Science
(Peer-Reviewed, Open Access, Fully Refereed International Journal)
Volume:05/Issue:10/October-2023 Impact Factor- 7.868 www.irjmets.com

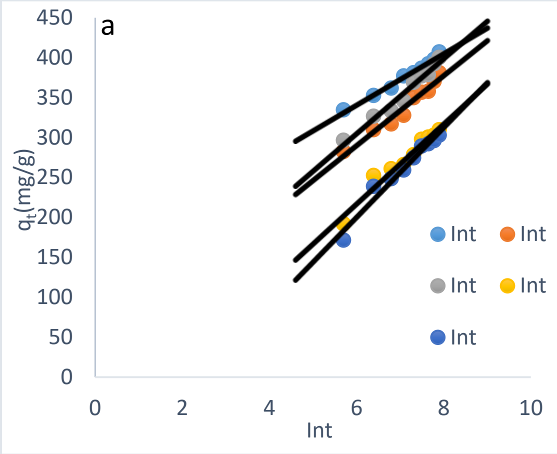

Fig. 6. Linear Elovich kinetic plot

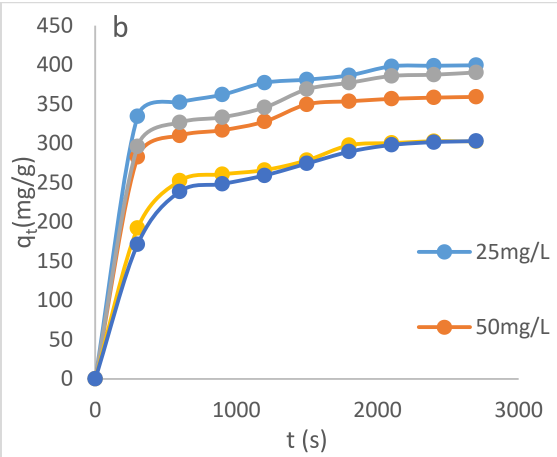

Fig. 7. Nonlinear Elovich kinetic plot.

Table 5: Intra-particle diffusion kinetic parameters.

Al																				
	25 mg/L				**50 mg/L**				**75 mg/L**				**100 mg/L**				**125 mg/L**			
t (s)	**D_p (m^2/s)**	**θ(mg/g)**	K_d(mg/g.$s^{-1/2}$)	**R^2**	**D_p (m^2/s)**	**θ(mg/g)**	K_d(mg/g.$s^{-1/2}$)	**R^2**	**D_p (m^2/s)**	**θ(mg/g)**	K_d(mg/g.$s^{-1/2}$)	**R^2**	**D_p (m^2/s)**	**θ(mg/g)**	K_d(mg/g.$s^{-1/2}$)	**R^2**	**D_p (m^2/s)**	**θ(mg/g)**	K_d(mg/g.$s^{-1/2}$)	**R^2**
300	1.2E-10				6.2E-11				6.4E-11				4.4E-12				1.7E-12			
600	7.3E-11				4.3E-11				4.5E-11				1.5E-12				9.3E-12			
9	5.3				3.1				3.2				1.2				8.1			

e-ISSN: 2582-5208
International Research Journal of Modernization in Engineering Technology and Science
(Peer-Reviewed, Open Access, Fully Refereed International Journal)
Volume:05/Issue:10/October-2023 Impact Factor- 7.868 www.irjmets.com

0 0	E-11				E-11				E-11				E-12				E-12	
1 2 0 0	4.6 E-11				2.5 E-11				2.7 E-11				1.0 E-12				7.7 E-12	
1 5 0 0	3.8 E-11	30 2. 7	1.9 91	0. 9 8 8 1	2.6 E-11	23 7. 4	2.7 36 8	0. 9 8 3	2.7 E-11	24 8. 4	2.9 39	0. 9 8 3	9.6 E-12	16 1. 1	3.0 18	0. 9 0 6 2	8.1 E-12	13 8. 1	3.3 76	0. 9 0 3 9
1 8 0 0	3.4 E-11				2.3 E-11				2.4 E-11				1.0 E-12				8.5 E-12			
2 1 0 0	3.1 E-11				1.9 E-11				2.3 E-11				9.2 E-12				7.6 E-12			
2 4 0 0	2.8 E-11				1.9 E-11				2.1 E-11				8.6 E-12				6.9 E-12			
2 7 0 0	2.8 E-11				1.9 E-11				1.9 E-11				8.0 E-12				6.8 E-12			

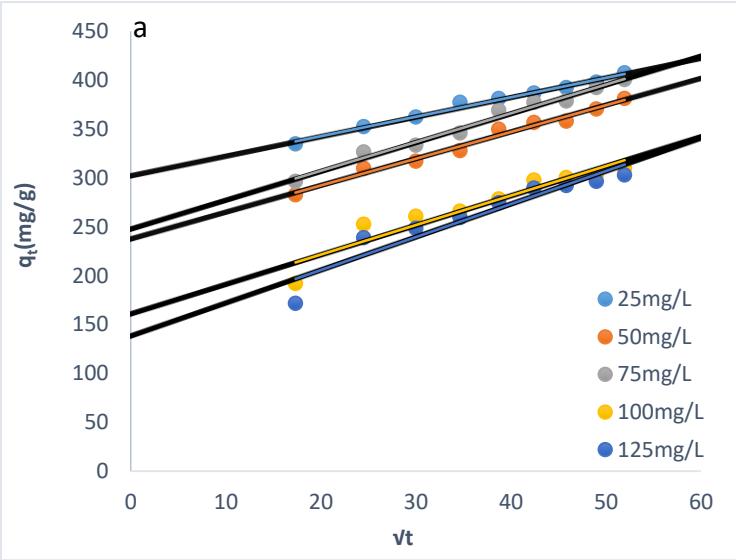

Fig. 8. Intra-particle diffusion kinetics.

e-ISSN: 2582-5208
International Research Journal of Modernization in Engineering Technology and Science
(Peer-Reviewed, Open Access, Fully Refereed International Journal)
Volume:05/Issue:10/October-2023 Impact Factor- 7.868 www.irjmets.com

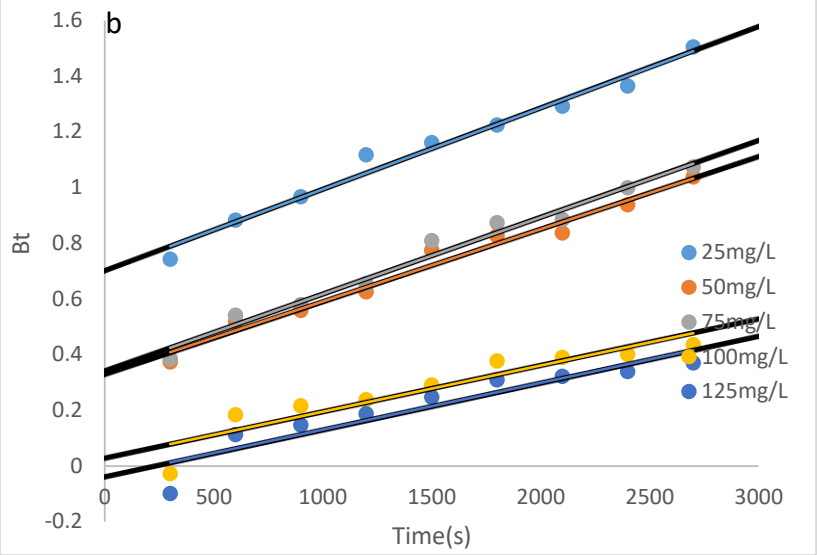

Fig. 9. Boyd-Reichenberg kinetic.

3.2 Adsorption isotherm

3.2.1. Langmuir isotherm

The Langmuir isotherm assumes monolayer deposition of adsorbate on the homogenous adsorbent surface. The mathematical expression of Langmuir isotherm is presented in Table 1.

The adsorption constant, b (L mg^{-1}) and the sorption capacity, q_o (mg g^{-1}) can be estimated by plotting C_e/q_e against C_e. The model simulations along with experimental observations for Langmuir isotherm are shown in Fig. 10. The values of the Langmuir constant, b, the adsorption capacity, q_o, and the regression coefficient, r^2 for linear are shown in Tables 6 and 7. The Langmuir isotherm can also be characterised in terms of the dimensionless constant separation factor, R_L (Eq. 20).

$$R_L = \frac{1}{1+bC_o} \qquad (20)$$

Where b (L/mg) is Langmuir constant and C_o (mg/L) is the initial concentration. The value of R_L indicated the nature of Langmuir isotherm to either unfavourable (R>1), favourable (0<R_L<1), Linear (R_L=1) or irreversible (R_L=0), [39]. The sorption process can also be described as favourable when b>0 [6].

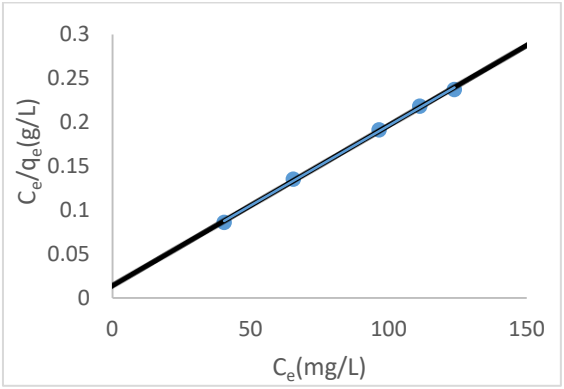

Fig. 10. Langmuir isotherm plot.

3.2.2. Dubinin-Radushkevich (D-R) isotherm

To calculate the sorption energy, the Dubinin-Radushkevich (D-R) model was used. This isotherm does not assume constant adsorption potential or homogeneous and heterogeneous surfaces [40]. It assumes that the characteristics of the sorption curves are related to the porosity of the adsorbent [36]. From the D-R isotherm, Inq_e is plotted against ε^2 from which q_s and β are determined from the intercept and slope respectively (Table 1). The regression coefficient r^2, the apparent sorption energy β, the theoretical saturation capacity q_s, and the Polanyi potential ε^2 for linear and nonlinear Dubinin-Radushkevich isotherm are summarized in Tables 6 and 7.

e-ISSN: 2582-5208
International Research Journal of Modernization in Engineering Technology and Science
(Peer-Reviewed, Open Access, Fully Refereed International Journal)
Volume:05/Issue:10/October-2023 Impact Factor- 7.868 www.irjmets.com

The model shows a similar value for q_o from Langmuir isotherm when compared to the q_s obtained using Dubinin–Radushkevich isotherm (Tables 6 and 7). The higher the values of q_s, the higher the sorption capacity and the better the biosorbents [41].

3.2.3. Temkin isotherm

The adsorption potential of adsorbate on adsorbent can be tested by applying the Temkin isotherm model [37]. The isotherm model (Temkin) takes into consideration the interaction between sorbent and adsorbent [6]. Both linear and nonlinear forms of Tempkin isotherm equations are presented in Table 1. From the plot of q_e against log C_e, the Temkin isotherm constants A and B can be calculated using the intercept and slope, respectively. The parameters of the isotherm and the regression coefficient (r^2) for the fitting of the experimental data are presented in (Tables 6 and 7).

3.2.4. Freundlich isotherm

The Freundlich adsorption isotherm is an empirical model relating the adsorption intensity of the sorbent towards the adsorbent [42]. The isotherm describes the multilayer adsorption with a heterogeneous energetic distribution of active sites, accomplished by the interaction between adsorbed molecules [38]. The linear and nonlinear mathematical expressions for the Freundlich mode are presented in Table 1. The Freundlich constant k_f which is a function of adsorption capacity, the energy or intensity of adsorption n (indicating the favorability of the adsorption process) and the regression coefficient R^2 values are presented in Tables 6 and 7. For n value less than one (n<1). It implies that the sorption process is a chemisorption while n values greater than one (n>1) indicated a favourable physical adsorption process [43]. The value obtained in this study suggests favourable physical adsorption (Tables 6 and 7) in which weak Van der Waals forces are dominant.

Table 6: Linear isotherm parameters at different temperatures.

Isotherm	T (K)	303	313	323	333
Langmuir	b (L mg^{-1})	0.1286	0.1006	0.0499	0.0536
	q_o (mg g^{-1})	555.56	555.56	555.56	555.56
	R_L	0.2372	0.2845	0.4449	0.4274
	r^2	0.9994	0.9996	0.9993	0.9988
Freundlich	K_f (mg g^{-1})	0.9266	0.9137	0.8645	0.8965
	1/n $(L/mg)^{-1}$	0.0901	0.1018	0.1453	0.0903
	r^2	0.9744	0.9877	0.993	0.9574
Temkin	A (L/mg)	920.3	225.05	8.46	401.09
	B	44.477	49.709	68.554	40.364
	r^2	0.97	0.9852	0.9921	0.9529
D-R	ε^2	86.2726	75.2018	63.7885	43.3959
	β (mol^2. $K J^{-2}$)	0.0012	0.0015	0.003	0.0024
	q_s (mol g^{-1})	539.85	540.12	545.88	486.77
	r^2	0.9184	0.9431	0.9777	0.9071

Table 7: Nonlinear isotherm parameters at different temperatures.

Isotherm	T (K)	303	313	323	333
Langmuir	b (L mg^{-1})	0.0497	0.02376	0.01132	0.00676
	q_o (mg g^{-1})	487.428	487.428	487.428	487.428
	R_L	0.4459	0.6274	0.7794	0.8554
	r^2	0.9999	0.9995	0.9984	0.9997
Freundlich	K_f (mg g^{-1})	0.2565778	0.234814	0.726806	0.199897

e-ISSN: 2582-5208
International Research Journal of Modernization in Engineering Technology and Science
(Peer-Reviewed, Open Access, Fully Refereed International Journal)
Volume:05/Issue:10/October-2023 Impact Factor- 7.868 www.irjmets.com

	1/n (L/mg)$^{-1}$	0.0801	0.1018	0.26085	0.1103
	r^2	0.9877	0.9865	0.9985	0.9648
Temkin	A (L/mg)	1110.3	225.05	102.0875	103.09
	B	81.477	87.709	91.09	86.364
	r^2	0.9848	0.9975	0.9899	0.9979
D-R	ε^2	41.1008	27.2018	36.7885	29.6206
	β (mol^2. K J^{-2})	0.00062	0.0015	0.00135	0.00236
	q_s (mol g^{-1})	493.85	494.12	495.88	498.51
	r^2	0.9399	0.9568	0.9376	0.9158

3.3. Adsorption thermodynamics

The thermodynamic effect of temperature on the adsorption process can be seen in Fig. 10. The ΔH, and ΔS for the adsorption process were calculated from the slope and intercept of Inb versus T^{-1} plot using Eq. 18 [44]. The ΔG is obtained from Eq. (17). The values of ΔG^0, ΔH^0 and ΔS^0 for the turbidity reduction using aluminium electrodes at different temperatures are given in Table 8. A positive value of enthalpy change (ΔH^0) indicates that the adsorption process is endothermic in nature while the negative value of Gibb's free energy (ΔG^0) shows the spontaneity and feasibility of the adsorption process [Majdi et al., 2016]. In addition, the positive value of (ΔS^0) indicates the increased disorder and randomness at the solid interface with the adsorbent. For E_a value below <8 KJ/mol, the adsorption process is physical [32] and if the E_a value is between 8 and 16 KJ/mol, the dominant mechanism is chemisorption [Argun et al., 2007]. Furthermore, adsorption may be dominated by particle diffusion if Ea>16 KJmol [47; 48]. In the present study, E_a values calculated are 20.4 and 18.26, 12.910, 14.433 KJ/mol at 303, 313, 323 and 333 K, respectively, which suggest that the mechanism of the adsorption process was mainly dominated by particle diffusion. This conforms with the previous work done by [48] on equilibrium adsorption modelling of lead (ll) on local clay minerals (NSU) from the aqueous stream.

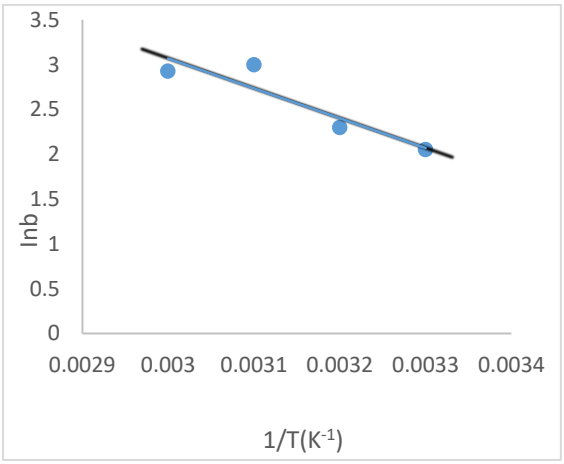

Fig. 11. Plot of ln$b$ against $\frac{1}{T}$.

Table 8: Thermodynamic and energy of adsorption at 303 K.

Temp(K)	ΔG^0(KJ/mol)	ΔH^0(KJ/mol)	ΔS^0(J/mol)	β	E_a(KJ/mol)
303	-5.1668	↓	↓	0.0012	20.400
313	-5.9774	27.6773	0.1085	0.0015	18.260
323	-8.0509	↑	↑	0.0030	12.910
333	-8.1036	↑	↑	0.0024	14.433

e-ISSN: 2582-5208
International Research Journal of Modernization in Engineering Technology and Science
(Peer-Reviewed, Open Access, Fully Refereed International Journal)
Volume:05/Issue:10/October-2023 Impact Factor- 7.868 www.irjmets.com

IV. CONCLUSION

The experiment was carried out to remove turbidity from simulated wastewater. Different adsorption kinetics such as pseudo-first order, pseudo-second order and Elovich, was investigated and the result showed that the pseudo-second-order kinetic offers a better description of the adsorption process. Also, the mechanism of the adsorption was studied using the intra-particle diffusion and the Boyd-Reichenberg model. The experimental data was also analysed using the adsorption isotherm such, as the Langmuir, Freundlich, Temkin and the Dubinin-Radushkevich. The adsorption process fitted well to the Langmuir isotherm, which suggested a monolayer coverage of adsorbed molecules. The adsorption thermodynamic study showed that the process is endothermic.

V. REFERENCES

[1] ATSDR. (2011). Agency for toxic substances and disease registry, centres for disease control and prevention. Available at htt://www.atsdr.cdc.gov.toxpro2.html.

[2] Hu, C.Y., Lo, S.L., Li, C.M., Kuan, W.H. (2005). Treating chemical mechanical polishing (CMP) wastewater by electro-coagulation-flotation process with surfactant. Journal of Hazardous Materials A120 (2005) 15–20.

[3] Muhammad, A.N., Zahira, Y., Ehsan, A., Ng, B.L., and Siti, R.S.A. (2013). A comparative study using aluminum and iron electrodes for the electrocoagulation of palm oil mill effluent to reduce its polluting nature and hydrogen production simultaneously. Pakistan J. Zool., vol. 45(2), pp. 331-337.

[4] Langmuir, I. (1918). The adsorption of gases on plane surface of glass, mica and platinum. Am Chem. Soc 40:1361–1403.

[5] Vasudevan, S., Lakshmi, J., Jayaraj, J., and Sozhan, G. (2009). Remediation of phosphate contaminated water by electrocoagulation with aluminium, aluminium alloy and mild steel anodes. Journal of Hazardous Materials 164: 1480–1486.

[6] Abideen, I.A., and Ramesh, B.B. (2015). Kinetics, isothermal and thermodynamics studies of electrocoagulation removal of basic dye rhodamine B from aqueous solution using steel electrodes. Appl Water Sci DOI 10.1007/s13201-015-0337-4.

[7] Olmez, T. (2009). The optimization of Cr(VI) reduction and removal by electrocoagulation using response surface methodology. Journal of Hazardous Materials, 162(2-3), 1371-1378.

[8] Chen, X., and Deng, H. (2012). Removal of humic acids from water by hybrid titanium-based electrocoagulation with ultrafiltration membrane processes. Desalination, 300, 51-57.

[9] Cañizares, P., Martínez, F., Rodrigo, M.A., Jiménez, C., Sáez, C., and Lobato, J. (2008). Modeling of wastewater electrocoagulation processes: Part I. General description and application to kaolin-polluted wastewaters. Separ. Purif. Tech. 60: 155-161.

[10] Balasubramanian, N., Kojima, T., and Srinivasakannan, C. (2009). Arsenic removal through electrocoagulation: kinetics and statistical modelling, chemical engineering journal 155: 76-82.

[11] Awad, Y.M., and Abuzaid, N.S. (2000). The influence of residence time on the anodic oxidation of phenol' separation and purification technology 18: 227-236.

[12] Heidmann, I., and Calmano, W. (2010). Removal of Ni, Cu and Cr from a galvanic wastewater in an electrocoagulation system with Fe and Al electrodes. Separ. Purif. Tech. 71: 308-314.

[13] Sridhar, R., Sivakumar, V., Prince Immanuel, V., and Prakash Maran, J. (2011). Treatment of pulp and paper industry bleaching effluent by electrocoagulation process. J Hazard Mater 186: 1495-1502.

[14] El-Nass, M.H., Al-Zuhair, S., and Al-Lobancy, A. (2009). Assement of electrocoagulation for the treatment of petroleum refinery wastewater' journal of environmental management 91: 180-185.

[15] Khenis, M., Tanguy, G., Leclerc, J.P., Valentine, G., and Lapicque, F. (2005). Electrocoagulation for the treatment of oil suspension: Relation between rates of electrode reactions and efficiency of waste removal' process safety and environmental protection 83: 50-57.

[16] Emamjomeh, M.M., and Sivakumar, M. (2009). Flouride removal by a continuous flow electrocoagulation reactor. Journal of environmental management 90: 1204-1212.

[17] Butler, E., Hung, Y.T., Yu-Li Yeh, R., and Al Ahmad, M.S. (2011). Electrocoagulation in wastewater treatment. Water 3: 495–525.

[18] Menkiti, M.C., Ugodulunwa, F.X.U., and Onukwuli, O.D. (2007). Studies on the coagulation and flocculation of coal washery effluent. Proceedings of the Nigeria Society of Engineers, 37: 169-184.

[19] Haghseresht, F., and Lu, G. (1998). Adsorption characteristics of phenolic compounds onto coal-rejected derived adsorbents, energy fuels 12: 1100-1107.

[20] Kumar, P.S., Ramakrishnan, K., and Kirupha, S.D. (2010). Thermodynamic and Kinetic studies of cadmium adsorption from aqueous solution onto rice husk. Braz. J. chem. Eng. vol. 27 no.2.

[21] Chen, X., Chen, G., and Yue, P.L. (2002). Investigation on the electrolysis voltage of electrocoagulation, Chem. Eng. Sci. 5: 2449–2455.

[22] Kucic, D., Markic, M., and Briski, F. (2012). Ammonium adsorption on natural zeolite (clinoptilolite): Adsorption isotherms and kinetics modelling.

[23] Rania, F., and Yousef, N.S. (2015). Equilibrium and kinetics studies of adsorption of copper (II) ions on natural biosorbent. International Journal of Chemical Engineering and Applications, vol. 6, No. 5.

[24] Wang, F.Y., Wang, H., and Ma, J.W. (2010). Adsorption of cadmium(ll) ions from aqueous solution by a new low-cost adsorbent-bamboo charcoal, Journal of hazardous materials, 177: 300-306.

[25] Kamaraj, R., Ganeson, P., Vasudevan, S., and Lakshmi. (2013). Removal of copper from water by electrocoagulation process – effect of alternating current (AC) and direct current (DC). Environ. sci. pollt. res.20: 399-412.

[26] Mall, I.D., Srivastava, W., and Argawal, K. (2006). Removal of orange G and Methyl Violet Dyes by Adsorption Onto Bagasse Fly Ash-Kinetic Study and Equilibrium Isotherm analyses, Dyes and Pigments, 69: 210-223.

[27] Maksin, D.D., Sladana, O.K., Maja, B.D., Jelena, P.M., Bojana, M.E., Antonije, E.O., and Aleksandra, B.N. (2012). Kinetic modelling of heavy metal sorption by vinyl pyridine based copolymer. Hem. Ind. 66: 795 -804.

[28] Karthikeyan, T., Rajgopal, S., and Miranda, L.R. (2005). Chromium(Vl) adsorption from aqueous solution by hevea brasiliensis sawdust activated carbon, J.hazard. Mater. 124: 192-199.

[29] Nwankwere, E.T., Gimba, C.E., Ndukwe, I.G., and Isuwa, K.A. (2015). Modelling of the kinetic and equilibrium sorption behaviour of crude oil on HDTMAB modified Nigerian nanoclays. International journal of scientific & technology research vol. 4, issue 02.

[30] Bajpai, S.K., and Jain, A. (2010). Removal of copper(II) from aqueous solution using spent tea leaves (STL) as a potential sorbent, water SA, vol. 36, no. 3, pp. 221-228.

[31] Ozer, A., and Dursun, G. (2007). Removal of methylene blue from aqueous solution by dehydrated wheat bran carbon. J. Hazard Mater. 146: 262-269.

[32] Balan, C., Volf, I., and Bilba, D. (2013). Chromium (VI) removal from aqueous solutions by purolite base anion-exchange resins with gel structure. 19: 615-628.

[33] Gholamreza, E.R., Hossein, A., Karim, Z., and Mehran, A. (2012). Adsorption of Ni(II) and Cd(II) ions from aqueous solutions by modified surface of typha latifolia L. root, as an economical adsorbent.

[34] Kumar, K.V., subanandam, K., Ramamurthi, V., and Sivanesan, S. (2005). Solid Liquid Adsorption for Wastewater Treatment: Principle Design and Operation. College Technology, Anna University, Chennai-India.

[35] Hamida, R., Ali, A.G., and Habibollah, Y. (2011). Isotherm and kinetics of Fe(II) adsorption onto chitosan in a batch process. International journal of energy and environment 2: 250-257.

[36] Tan, I.A., Hameed, B.H., and Ahmed, A.L. (2007). Equilibrium and kinetic studies on basic dye adsorption by oil palm fibre activated carbon. Eng. J. 12: 111-119.

[37] Zohre, S., Ataallah, S.G., and Mehdi, A. (2010). Experimental study on methylene blue adsorption from aqueous solution onto carbon Nano Tubes. Inter. J. of water and environ. Eng. vol. 2: 016-028.

[38] Chithra, K., and Balasubramanian, N. (2010). Modeling electrocoagulation through adsorption kinetics, J. of modeling and simulation of systems. Vol.1. Issue. 2: 124-130.

[39] Jafar, A. A., and Shajudha, A.B. (2012). Adsorption of copper from aqueous solution using low cost adsorbent. Archives of Applied Science Research, 4:1532-1539.

[40] Rondon, W., Freire, D., de Benzo, Z., Sifontes, A.B., Gonzalez, Y., Valero, M., and Brito, J.L. (2010). Application of 3A zeolite prepared from venezuelan kaolin for removal of Pb(ll) from wastewater and its determination by flame atomic absorption spectrometry. American journal of analytical chemistry. 4: 584-593.

[41] Chan, H., Zhao, J., Dai, G., Wu, J., and Yan, H. (2010). Adsorption characterstics of Pb (ll) from aqueous solution onto a natural biosorbent, Fallen Cinnamomum camphora leaves. Desalination, 262: 174-182

[42] Vasudevan, S., Lakshmi, J., and Sozhan, G. (2011). Effects of alternating and direct current in electrocoagulation process on the removal of cadmium from water. Journal of Hazardous Materials. 192: 26-34.

[43] Folasegun, A.D., and Kovo, G.A. (2014). Abstraction of Zinc (II) Ions from Solution unto a Nigerian Bentonite. The Pacific Journal of Science and Technology. Vol. 15. No. 1.

[44] Mohan, D., and Singh, K.P. (2002). Single-and multi-component adsorption of cadmium and zinc using activated carbon derived from bagasse: an agricultural waste, water res. 36: 2304-2318.

[45] Majdi, M.R., Danaee, I., and Nikmanesh, S. (2016). Kinetic and thermodynamic investigations on the electrocoagulation of methyl orange from aqueous solution using aluminum electrodes Bulgarian Chemical Communications. vol. 48, no, 4: 628-635.

[46] Singha, A.S., and Guleria, A. (2014). Chemical modification of cellulosic biopolymer and its use in removal of heavy metal ions from wastewater. International journal of biological macromolecules 67: 409-417.

[47] Argun, M.E., Sukru, D., Celalettin, O., and Mustafa, K. (2007). Heavy metal adsorption by modified oak sawdust: Thermodynamics and kinetics. Journal of Hazardous Materials 141: 77-85.

[48] Etukudoh, A.B., Akpomie, K.G., Obi, N.D., Agbo, A.E., and Chimezie, P.E. (2016). Equilibrium adsorption modelling of lead (ll) on local clay mineral (NSU) from aqueous stream. Int. Journal of Multidisciplinary Science and Engineering. vol. 7, no. 5: 22-25.

[49] Ho, Y.S. (2006). Second order kinetic model for the sorption of cadmium onto tree fern: A comparison of linear and nonlinear methods. Water research 40: 119-1.